Catalysis Science & Technology

Accepted Manuscript

ROYAL SOCIETY OF CHEMISTRY

www.rsc.org/catalysis

Cooperation between the surface hydroxyl groups of Ru-SiO_2@mSiO_2 and water for good catalytic performance for hydrogenation of quinoline

Colour graphic:

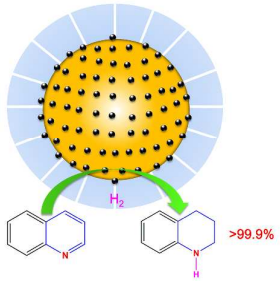

A new core-shell catalyst showed excellent performance and stability was used in the hydrogenation of quinoline in water.

Journal Name RSCPublishing

ARTICLE

Cite this: DOI: 10.1039/x0xx00000x

Received 00th January 2012,
Accepted 00th January 2012

DOI: 10.1039/x0xx00000x

www.rsc.org/

Cooperation between the surface hydroxyl groups of Ru-SiO_2@mSiO_2 and water for good catalytic performance for hydrogenation of quinoline

Lei Zhang,[a] Xiaoyan Wang,[b] Ying Xue,[a] Xiaojun Zeng,[a] Hua Chen,[a] Ruixiang Li,[a]* Shanling Wang[b]*

Abstract A well dispersed core-shell nanocatalyst Ru-SiO_2@mSiO_2 with Brunauer-Emmet-Teller surface area (S_{BET}) as high as 602 m^2/g has been prepared by a modified Stöber method and characterized by SEM, TEM, SAXRD and solid-state NMR. The catalyst shows an good catalytic performance for the hydrogenation of quinoline to 1,2,3,4-tetrahydroquinoline under mild condition in water. Both the conversion and selectivity are up to 100%. Furthermore, the catalyst could be recycled for five times without loss of both the activity and selectivity. It is postulated that the high performance of the novel catalytic system is related to the cooperation between the surface hydroxyl groups of microporous shell of Ru-SiO_2@mSiO_2 and water as solvent.

1. Introduction

The study on preparation of heterogeneous catalysts which are usually prepared by impregnating the metal salt or metal complex on the supports, such as carbon nanotubes, ZrO_2, Al_2O_3, SiO_2, collagen fibers, polymeric mesoporous carbon graphitic nitrides (mpg-C_3N_4) and ordered mesoporous graphitic carbon nitrides (ompg-C_3N_4) [1-8], is an important subject in chemical investigation. Unfortunately, the metal nanoparticles often migrate to the outer surface of the supports, which cause a worse metal distribution. And, the metal nanoparticles may be leached into the solution easily due to the weak interaction between the metal and the support. [9] To protect the metal nanoparticles from aggregating and leaching of the catalyst, an attractive conceptual design was core-shell catalysts, which is of great interests for chemists. [10] Recent reports revealed some interesting results in core-shell catalysts, Au@SiO_2, Au-Fe_3O_4@SiO_2, and Ag@Pd satellite-Fe_3O_4 facilitated the reduction of nitro compounds in the presence of $NaBH_4$. [11-13] Fe_3O_4@SiO_2-Au@mSiO_2, Au/TS-1@mSiO_2, and Pd/SiO_2@TiSS achieved the epoxidation of olefins and oxidation of sulfide efficiently. [14-16] Pt-SiO_2@TiO_2 displayed a highly thermal stability in the oxidation of CO. [17] Metallodendritic core-shell γ-Fe_2O_3 nanoparticles with an excellent reusability was used in Suzuki coupling. [18] Pd@CeO_2/functionalized-Al_2O_3 exhibited an exceptional activity for methane combustion. [19] The synthesis of 1,2,3,4-tetrahydroquinoline (^{1}THQ) and its derivatives have attracted considerable attention due to their important biological activation. [20] For their construction, the catalytic hydrogenation of quinoline over a supported catalyst has been demonstrated as an efficient strategy. However, the deactivation of catalyst, which was caused by the poison of quinoline and its hydrogenation products, [21] is usually the frustrating problem.

In our previous work, the cooperation between the surface hydroxyl groups of the supports and water (solvent) was found to play an important role to improve catalytic performance in the hydrogenation of *p*-chloronitrobenzene over Ir/ZrO_2·xH_2O [22], ester and citral over Ru/AlO(OH). [23, 24] However, the recycle of those catalysts was not satisfactory because of the hydrophobic metals on the surface of the supports. For the sake of creating the hydrophilic metal surface to improve the further performance and stability of the catalyst, we designed a core-shell nanocomposite catalyst with abundant surface hydroxyl groups. Herein, a facile strategy for the synthesis of Ru-SiO_2@microporousSiO_2 (Ru-SiO_2@mSiO_2) in two steps is presented. As expected, Ru-SiO_2@mSiO_2 catalyst shows an unprecedented selectivity and reusability in the hydrogenation of quinoline. Furthermore, Water used as the solvent in this catalytic system is a green processing which could reduce the environment pollution which fulfills the majority of the "Green Chemistry" requirements which impose environment friendly reagent.

2. Experimental

2.1 The preparation of catalyst

2.1.1 Chemicals:

Sodium borohydride, hexadecyl trimethyl ammonium bromide (CTAB) (99%), ethanol (>99%), ammonia solution (28% in

H_2O), quinoline and *p*-chloronitrobenzene (97%) were purchased from Sinopharm Chemical Reagent Co., Ltd, $RuCl_3 \cdot xH_2O$ (>37% in Ru) from Kunming Precious Metals Co., and tetraethoxysilane (TEOS) (98%) from Alfa Aesar. Deionized water (Millipore) with a resistivity of 18 MΩ·cm was used in all of the experiments. All reagents were used directly except quinoline, quinoline was distilled before use.

2.1.2 Synthesis of the catalyst

The silica nanospheres were firstly synthesized by a modified Stöber method. [25] Typically, 1.5 mL TEOS was added into a mixed solvent consisted of 0.5 mL $NH_3 \cdot H_2O$, 25 mL ethanol and 2.0 mL deionized water and stirred for 6 h. Next, 40 mg Ru^{3+} (5 mg/mL in ethanol) was added and the stirring continued for another 3 h. Subsequently, 5.0 mL $NaBH_4$ solution was dropped into the suspension to reduce the Ru^{3+}. The suspension was filtered and dried in vacuum at room temperature. The product was denominated as Ru-SiO_2.

Ru-SiO_2 (250 mg) and CTAB (450 mg) were dispersed in the mixed solvent including 150 mL ethanol and 100 mL deionized water. Then, 2.0 mL $NH_3 \cdot H_2O$ and 1.5 mL TEOS was injected and stirred for 6 h. The product was filtered and dispersed in the refluxing solution containing 200 mL ethanol and 1.5 mL concentrated hydrochloric acid to remove the CTAB. The solid was collected and washed by ethanol and dried in vacuum. The product was denominated as Ru-SiO_2@mSiO_2. The preparation routes of the Ru-SiO_2@mSiO_2 was summarized in Scheme 1.

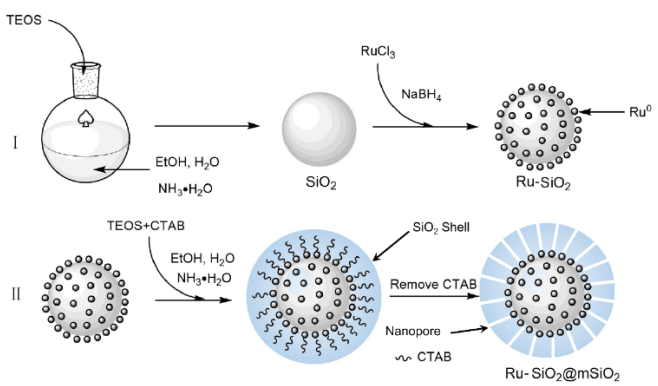

Scheme 1 The synthetic route to Ru-SiO_2@mSiO_2

2.2 Characterization of the catalyst

Ru loading amount in the catalyst was determined by an inductively coupled plasma atomic emission spectrometer (ICP-AES, Varian VISTA-MPX). Fourier transform infrared (FTIR) spectra were collected in a NEXUS670FT-IR spectrometer. SEM images were obtained from JEOL JSM-7500F microscope. TEM and high-angle annular dark-field scanning transmission electron microscopy (HAADF-STEM) images were carried out in Tecnai G^2 F20. Energy-dispersive X-ray analysis (EDAX) was done in the middle of the selected particles. Low-angle XRD was recorded with SAX X'TRA spectrometer in the angle region from 0.5° to 6° with a step of 0.01°. X-ray photoelectron spectroscopy (XPS, Kratos XSAM-800, UK) analyses were conducted by employing Mg Kα X radiation (hν = 1253.6 eV), all the binding energy peaks of XPS spectra were calibrated with C1s binding energy peak at 284.7 eV. BET was recorded on Quadrasorb SI. The sample was degassed till the residual presure less than 10^{-4} Pa at 353 K for 3 h. Barrett-Joyner-Halenda (BJH) method was used to calculate the pore distribution. ^{13}C NMR spectra was recorded on a Bruker AV II-600 MHz spectrometer with the D1 time of 2.00 s in $CDCl_3$. Solid-state ^{29}Si MAS NMR and solid-state ^{13}C MAS NMR spectra were recorded on a Bruker AVANCE III 500MHz spectrometer with the D1 time of 5.00 s.

The hydrogenation products were detected by gas chromatography (GC) with the HP-5 (30 m×0.5 mm×0.25 μm) column and flame ionization detector (FID). All the components were confirmed by gas chromatography-mass spectrometry (GC-MS).

2.3 Catalytic test and recycling in quinoline hydrogenation

In general, the molar ratio of substrate to metal was chosen as 150 to test the catalytic performance. A typical reaction condition was described as follows: 1.0 mmoL quinoline, 2.0 mL solvent and appropriate amount of the catalyst (about 35 mg) were transferred to a Teflon-lined autoclave and the hydrogen was charged to the desired pressure after removing the air. After the autoclave was heated to 363 K in about 25 min (the conversion of quinoline during the heating time was detected as low as about 3.6%, which could be neglected) (Detail of the experiment is available in ESI) , the stirring and time counting were started. When the reaction finished, all the products were taken out and the autoclave was washed with ethanol for 3 times (3.0 mL×3) to collect the products. The catalyst was separated by centrifugation. The liquid phase was analyzed by GC. For the recycling test, the catalyst was recovered by centrifugation, washed with ethanol (1.0 mL ×3) for three times, and dried under vacuum at 323 K for 5 h.

3. Results and discussion

3.1 Catalyst characterization

FTIR spectra confirmed the CTAB in Ru-SiO_2@mSiO_2 was removed successfully (Fig. S1; ESI). SEM images of Ru-SiO_2@mSiO_2 in Fig. 1A showed the well-dispersed smooth spheres with the average diameter of 660 nm were obtained (Fig. S2; ESI) after silica coating, and the core-shell structure was clearly observed in Fig. 1B.

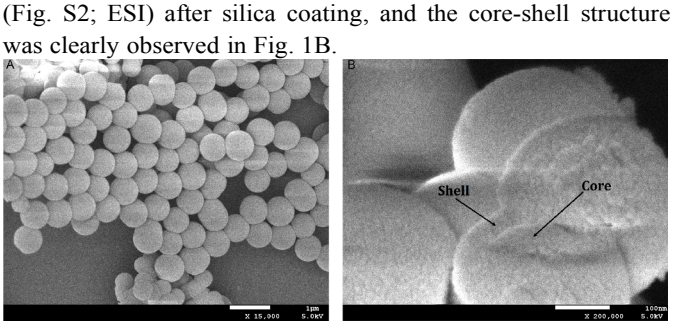

Fig. 1 SEM image of Ru-SiO_2@mSiO_2 particles
The length of the side bar is 1μm in A, while it is 100 nm in B

Fig. 2 showed bright-field TEM images (A and B) and HAADF-STEM (C and D) images of Ru-SiO_2 and Ru-SiO_2@mSiO_2. The TEM observation indicated that the average diameter of Ru nanoparticles was 6.4 nm and Ru nanoparticles had no aggregation (Fig. 2A and Fig. 2E). The Ru-SiO_2 was coated well by the microporous silica layer with the thickness of 90 nm (Fig. 2B). The HAADF-STEM image (Fig. 2C and Fig. 2D) and EDXA spectra (Fig. S3; ESI) also demonstrated that Ru nanoparticles were well dispersed on the surface of the SiO_2 spheres and the Ru nanoparticles were successfully immobilized in the nanocomposite. High resolution electron microscopy (HRTEM) images of Ru nanoparticles on the surface of Ru-SiO_2 and their Fast Fourier Transformation (FFT) (Fig. S4; ESI) illustrated that the Ru nanoparticles were amorphous. Low-angle XRD pattern of Ru-SiO_2@mSiO_2 in Fig. S5 (ESI) displayed a broad diffraction peak at around 2.5°, which was assigned to the reflection of a 2-D hexagonal mesostructure, [14] also indicating a worm like micropore with a uniform pore size.

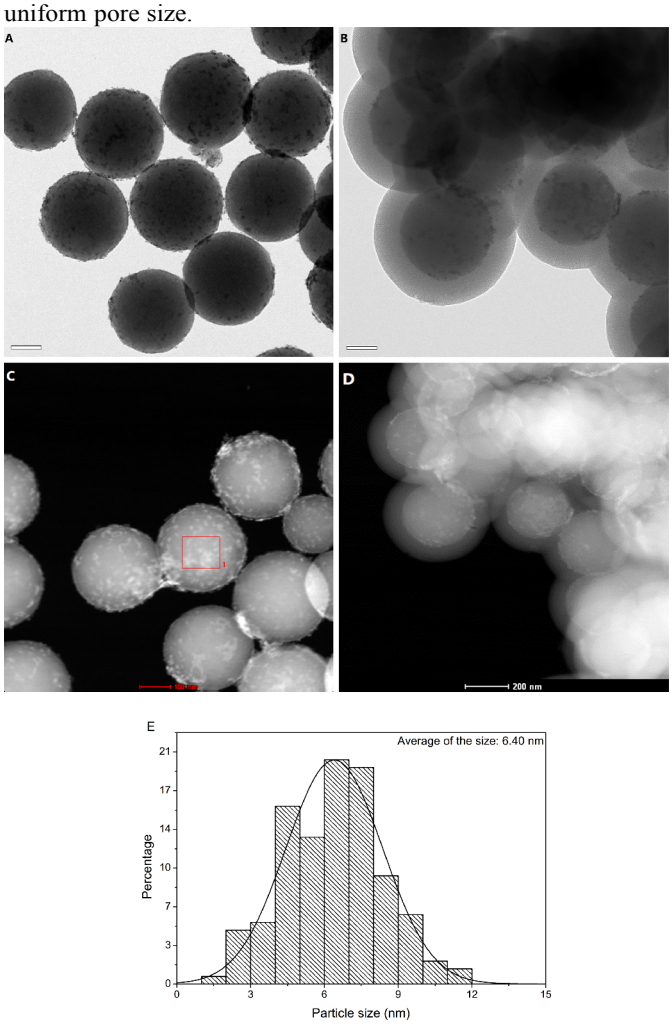

Fig. 2 TEM images of the Ru-SiO_2 and Ru-SiO_2@mSiO_2 (A and B), HAADF-STEM images of the Ru-SiO_2 and Ru-SiO_2@mSiO_2 (C and D), and size distribution of Ru nanoparticles (E)

The length of the side bar is 100 nm in A, B, and C, while it is 200 nm in D

Solid-state ^{29}Si cross polarization/magic angle spinning (CP/MAS) NMR spectra of Ru-SiO_2@mSiO_2 in Fig. 3 exhibited the strong shift values at -90.8/-102.1/-111 ppm for $Q^2/Q^3/Q^4$ signals (Q^2: $\{(HO)_2Si(OSi)_2\}$, Q^3: $\{(HO)Si(OSi)_3\}$, Q^4: $\{Si(OSi)_4\}$). [26] The presence of the strong Q^2 - Q^3, and weak Q^4 signals in Ru-SiO_2@mSiO_2 suggested that the nanocomposite possessed main structures of $\{(HO)Si(OSi)_3\}$ and $\{(HO)_2Si(OSi)_2\}$, which could give a conclusion that abundant hydroxyl groups on the surface of the catalyst are present.

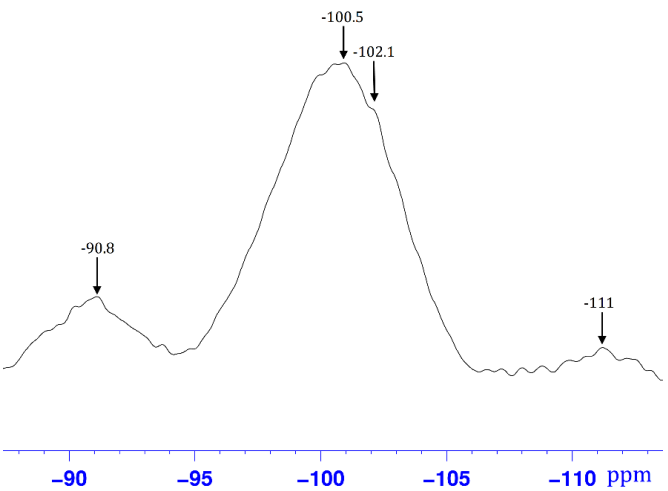

Fig. 3 Solid-state ^{29}Si CP/MAS NMR spectra of Ru-SiO_2@mSiO_2

Specific surface area (S_{BET}) of Ru-SiO_2@mSiO_2 was characterized by BET method using N_2 adsorption-desorption. The adsorption-desorption of the microspheres showed the representative type-IV curves (Fig. S6A, ESI) which suggested cylindrical pores with a narrow distribution at 1.1 nm (Fig. S6B, ESI). The BET surface area and the total pore volume were calculated as 602 m^2/g and 0.32 m^3/g, respectively.

The metal content in the Ru-SiO_2@mSiO_2 (2.0 wt% for Ru) was determined by the ICP-AES. The oxidation state of Ru was detected by XPS and shown in Fig. S7 (ESI). The survey spectra of Ru-SiO_2@mSiO_2 in Fig. S7A confirmed the composition of the catalyst. The doublets observed at 281.9 and 285.1 eV in the Ru 3d XPS spectra of Ru-SiO_2@mSiO_2 in Fig. S7B was higher than 280.1 eV and 285.0 eV of Ru^0, [27] which indicated the oxidation state of the Ru nanoparticles in Ru-SiO_2@mSiO_2 was $Ru^{\delta+}$.

3.2 Hydrogenation of quinoline

Mass transfer limitation would lead to the less conversion due to the poor solubility of substrate or the poor diffusion of the substrate from the surface of the catalyst to the active

centers. The conversion of quinoline in different stirring rate (Fig. S8, ESI) showed the conversion of quinoline was 15.5% with the selectivity to ^{1}THQ as high as 100% at the stirring rate of 400 rpm. However, the reaction was accelerated and gave the conversion 80% when the stirring rate was set at 1200 rpm or higher. To overcome the mass transfer limitation, we set the stirring rate at the constant of 1500 rpm in the further study.

3.2.1 The effect of solvent on the hydrogenation of quinoline

The hydrogenation of quinoline generally forms three products 1,2,3,4-tetrahydroquinoline (^{1}THQ), 5,6,7,8-tetrahydroquinoline (^{5}THQ), and decahydroquinoline (DHQ) as shown in Scheme 2.

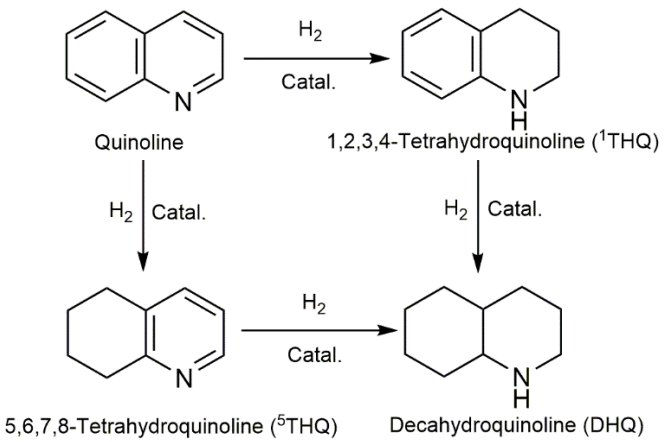

Scheme 2 Possible pathways for hydrogenation of quinoline

In homogeneous catalytic system, the free energy state of the reactants could be changed due to the difference of the solvent-electronic properties, which can alter the mechanistic aspects in a reaction. In other words, the nature of the solvent can alter the mechanism paths in different reactions. In heterogeneous catalytic system, the impact of solvents on the overall mechanism is still not to be understood clearly. However, the studies on the effect of solvent on reaction indicated that the polar solvent was preferred in the hydrogenation of the weak polar reactants. [28, 29] In this catalytic system, the performance of the catalyst for the hydrogenation of quinoline in different solvents is displayed in Table 1. Under the conditions of 363 K, 3.0 MPa hydrogen pressure and 5 h reaction time, quinoline was completely converted with 100% selectivity toward ^{1}THQ in water. The conversion of quinoline decreased in the following order: water > ethanol > *i*-propanol > tetrahydrofuran > toluene > 1,4-dioxane, which was consistent with the polarity order of the solvents. This phenomenon was also observed in the hydrogenation of quinoline over palladium supported on tannin grafted collagen fibers (Pd-BT-CF) and Ru/P4Vpy (P4Vpy = Polyvinylpyridine).[7, 30] These results suggested that the increase of the solvent polarity was beneficial for the hydrogenation of quinoline over Ru-SiO_2@mSiO_2

Table 1 Conversion of quinoline in different solvent

Solvent	Conv. (%)[a]	Sel. (%)[a]		
		^{1}THQ	^{5}THQ	DHQ
Water	100	100	0	0
Ethanol	87.5	95.8	3.1	1.1
i-Propanol	75.3	95.3	4.0	0.7
Tetrahydrofuran	55.7	85.4	9.2	5.4
Toluene	45.8	88.7	7.2	4.1
1,4-Dioxane	25.3	96.3	2.6	1.1

Reaction conditions: quinoline (1.0 mmoL), Ru (0.67 mol% relative to quinoline), 2.0 mL solvent, 363 K reaction temperature, 3.0 MPa hydrogen pressure, 5 h reaction time.

3.2.2 The effect of hydrogen pressure and reaction time on the hydrogenation of quinoline

The effect of the hydrogen pressure and reaction time in the hydrogenation of quinoline was illustrated in Table 2. The conversion of quinoline was only 23.7% with the selectivity as high as 100% to ^{1}THQ (Entry 1 in Table 3) at the low hydrogen pressure (0.5 MPa). The conversion was improved rapidly with increase of the hydrogen pressure without any loss of the selectivity. Both the conversion of quinoline and selectivity to ^{1}THQ were up to 100% at 2.0 MPa (Table 3, Entry 3). Although the diffusion of the quinoline from the shell surface to the active metal centers on core slowed down the rate of the hydrogenation in this catalytic system because of 90 nm's thickness of the shell (Fig. 2B) with the pore diameter about 1.1 nm while the kinetic diameter of quinoline is about 0.65 nm, the conversion and selectivity were higher than that obtained over 10% Ru/P4Vpy at 4.0 MPa and 393 K. [30] Those results demonstrated the high activity of this new catalyst. Interestingly, although the hydrogen pressure or the reaction time was further increased, ^{1}THQ could not be hydrogenated to DHQ when the conversion of quinoline reached 100%. Based on Fish's research, [31] the product distribution of hydrogenation of quinoline depends on the adsorption types of quinoline over a catalyst. The quinoline absorbed on the catalyst through the coordination of nitrogen atom favors to produce ^{1}THQ (Scheme 3A) and the adsorption of phenyl ring leads to the formation of ^{5}THQ (Scheme 3B).

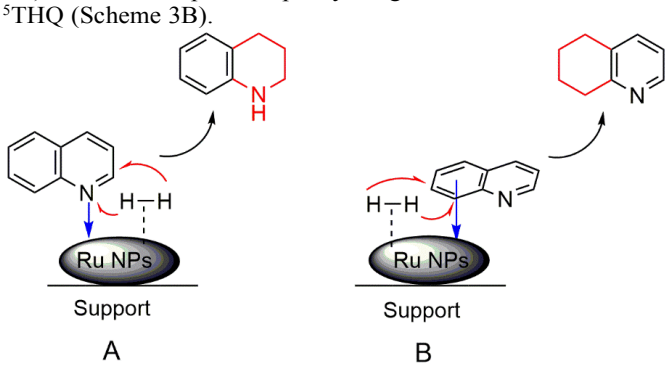

Scheme 3 the influence of product in hydrogenation of quinoline by the adsorption type on Ru nanoparticles

Therefore, the effect of solvents, hydrogen pressure and reaction time in this catalytic system indicated that quinoline was only adsorbed via nitrogen atom coordination with ruthenium center in water.

Table. 2 The influence of hydrogen pressure and reaction time on the hydrogenation of quinoline

Entry	Pressure (MPa)	Reaction Time (h)	Con. (%)	Sel. to ^{1}THQ (%)
1	0.5	5	23.7	100
2	1.0	5	79.3	100
3	2.0	5	100	100
4	3.0	5	100	100
5	4.0	5	100	100
6	5.0	5	100	100

7	3.0	1	20.5	100
8	3.0	2	37.8	100
9	3.0	3	79.4	100
10	3.0	4	83.2	100
11	3.0	5	100	100
12	3.0	6	100	100

Reaction conditions: 1.0 mmoL quinoline, Ru, 0.67 mol% relative to quinoline; 2.0 mL water, 363 K reaction temperature.

3.2.3 The reusability of the catalyst

Recycle ability of a catalyst is one of the most important issues in the practical application. Some works revealed that catalysts used in the hydrogenation of quinoline are very difficult to be recycled [30, 32] due to the strong coordination ability of nitrogen atom in quinoline and its hydrogenation products, which leads to the quick loss of the catalytic activity. In other catalytic system, protonic acid and special additives were often added to the hydrogenation system to prevent the catalyst from the poison of nitrogen atom. [33] However, the addition of protonic acid would cause the corrosion of the equipment and additives would lead to the difficulty in the product separation. In this work, no additives were added to the catalytic system, the Ru-SiO_2@mSiO_2 catalyst could be recycled five times without any loss of catalytic activity and selectivity (Fig. 4). After the 6th catalytic cycle, the conversion of quinoline declined from 100% to about 73.6%. After 12 catalytic cycles finished, only 35.2% conversion of quinoline was obtained, however, the selectivity to ^{1}THQ always remained to be 100% through the 12 catalytic cycles. Obviously, this catalytic system showed an unprecedented ability to resist the poison from nitrogen atom in quinoline and its hydrogenation derivatives.

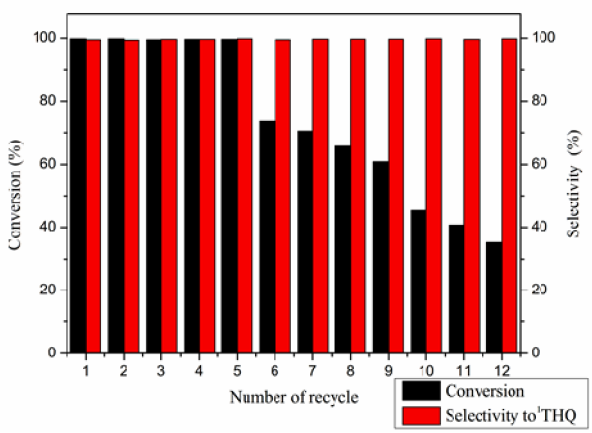

Fig. 4 Recycle of Ru-SiO_2@mSiO_2 catalyst in hydrogenation of quinoline

ICP-AES analysis found that the total leaching amount of ruthenium was 0.04% after 5 catalytic cycles, which indicated that the Ru leaching was inhibited efficiently in this catalytic system. Meanwhile, we proved that the leached ruthenium was not the active species in the hydrogenation of quinoline. (Table S1, details of the experiments are available in ESI). Furthermore, TEM (Fig. 5A) indicated that after the 5 catalytic cycles, no obvious aggregation of Ru nanoparticles were observed due to the isolation role of the shell for Ru nanoparticles on the core, however, after 12 catalytic cycles, the Ru nanoparticles was obtained a little aggregation in the TEM image (Fig. 5B). S_{BET} of the catalyst used for 5 catalytic cycles was tested as 285 m^2/g while further decreased to 138 m^2/g after 12 catalytic cycles, which was much lower than the fresh catalyst (602 m^2/g). The result showed the microporous shell of the catalyst was destroyed, which could slow down the diffusion of the quinoline to contact with the Ru nanoparticles on core in the reaction.

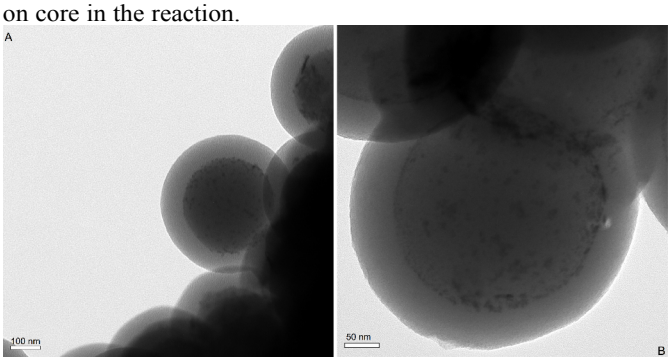

Fig. 5 TEM image of Ru-SiO_2@mSiO_2 after 5th recycle (A) and 12th recycle (B)

3.2.4 Comparison with other catalysts

Ru/SiO_2 and Ru/SiO_2-spheres were prepared to compare the catalytic performance of Ru-SiO_2@mSiO_2. The results are illustrated in Table 3. Ru/SiO_2 gave only 55.3% conversion with the 82.7% selectivity to ^{1}THQ, and its catalytic activity and selectivity in the second use decreased to 20.3% and 75.4%, respectively. For Ru/SiO_2-spheres catalyst, quinoline conversion increased to 98% and the selectivity was a little higher than that over Ru/SiO_2, but the activity of Ru/SiO_2-spheres catalyst rapidly decreased to 62.3% and the selectivity to ^{1}THQ decreased to 74.0% in the third use. The fresh NanoRu@hectorite catalyst could give the full conversion of quinoline to ^{1}THQ in water (30 bar H_2, 373K), the activity would be lost very quickly in the second use (Table 3). [33] Also, the commercial Pd@C catalyst can only obtain about 80% conversion and lost its activity very quickly in the hydrogenation of quinoline in the second catalytic cycle (2.0 MPa, 333K). [34] No matter higher or lower conversion of quinoline, it gave 100% selectivity to ^{1}THQ over Ru-SiO_2@mSiO_2 catalyst in water (Table 2 and Table 3). Obviously, the catalytic performance of Ru-SiO_2@mSiO_2 was the best among the investigated catalysts. Compared with catalyst Pd@C, Ru/SiO_2, and Ru/SiO_2-spheres, the main difference of Ru-SiO_2@mSiO_2 is that there are abundant hydroxyl groups on the surface of the core as well as on the surface of shell based on the results of ^{29}Si CP/MAS NMR. The results revealed that the activity and selectivity in our catalytic system were related to the surface hydroxyl group numbers on the catalysts closely.

Table 3 The Hydrogenation of quinoline over different catalysts

Catalyst	Conversion (%)	Selectivity (%)	
		^{1}THQ	^{5}THQ
Ru/SiO_2[a]	55.3	82.7	17.3
	20.3	75.4	24.6
Ru/SiO_2-Spheres[b]	98.0	87.5	12.5
	87.2	80.3	19.7
	62.3	74.0	26.0
Ru-SiO_2@mSiO_2[a]	100	100	0

NanoRu@hectorite	99.6	>99.0	<1.0
	23	>99.9	0

Reaction conditions: 1 mmoL quinoline, Ru, 0.67 mol% relative to quinoline; 2.0 mL water, 363 K reaction temperature, 3.0 MPa hydrogen pressure, [a], 5 h reaction time, [b], 3 h reaction time.

Note: SiO_2 was commercially available with the size distribution about 300-400 meshes; SiO_2-spheres were synthesized by Stöber method with the size distribution about 480 nm. The detail synthesis of the two catalysts were described in the ESI.

3.2.5 Possible catalytic mechanism in the hydrogenation of quinoline

In this catalytic system, ^{1}THQ is only product through the entire range of the reaction conditions. The results in Table 2 indicated that water played an important role to obtain ^{1}THQ selectively. In other words, quinoline was adsorbed through nitrogen atom over Ru-SiO_2@mSiO_2 in water, while both adsorption types were present in organic solvent (Scheme 3). Furthermore, the comparison of the hydrogenation results over Ru/SiO_2-spheres with that over Ru-SiO_2@mSiO_2 (in Table 4) indicated that the existence of SiO_2 shell was a key factor to give the high selectivity to ^{1}THQ. N_2 adsorption-desorption isotherms in Fig. 4A and low-angle XRD revealed that the catalyst was of a worm-like micropore with a uniform pore size. Accordingly, the water as solvent and the microporous structure of the shell caused the cooperation for the highly selective hydrogenation of quinoline. Additionally, abundant hydroxyl groups on the surface of SiO_2 shell and core were present according to ^{29}Si CP/MAS NMR spectra of Ru-SiO_2@mSiO_2 in Fig. 3, which formed the highly hydrophilic surface. When water was used as the solvent, it was suggested that a water film was formed on the hydrophilic surface of Ru-SiO_2@mSiO_2.[35] Hence, the nitrogen atom in quinoline molecule could adsorb on the surface of the catalyst selectively via the hydrogen bond as well as the coordination with metal active species. Meanwhile, the adsorption of phenyl ring was inhibited on active metal sites due to the hydrophobic phenyl ring part of quinoline molecule. All the factors result in the high selectivity to ^{1}THQ achieved in this catalytic system. As a comparison, quinoline could be adsorbed on the metal surface via the coordination of phenyl ring as well as nitrogen atom with metal. These factors result in the products of ^{1}THQ and ^{5}THQ in organic solvents (Table 1).

Compared with Ru-SiO_2@mSiO_2, Ru/SiO_2-spheres and Ru/SiO_2 are also hydrophilic, which caused the high selectivity to ^{1}THQ. However, the Ru particles on the surface of the supports do not contain hydrophilic groups, quinoline could be adsorbed on the active metal surface via route B (Scheme 3B) to give ^{5}THQ because of unstable water film on metal surface. The key of this work is to design the catalyst and changes the hydrophobic metal surface to be hydrophilic. We prepared Ru-SiO_2@mSiO_2 catalyst and utilize the uniform microporous structure as well as abundant surface hydroxyl groups of SiO_2 shell. In this catalyst, the most surfaces of Ru nanoparticles are surrounded with hydroxyl groups, when Ru nanoparticles are embedded between core and microporous shell of SiO_2 (Scheme 4). In this case, the surface of Ru nanoparticle is of good hydrophile. As expected, Ru-SiO_2@mSiO_2 catalyst shows the high selectivity to the formation of ^{1}THQ in water because N-heterocycle is selectively adsorbed on the metal surface via the hydrogen bond between nitrogen atom of quinoline molecule and hydroxyl group. The hydrogen bond does not only improve the catalytic selectivity, but also significantly weaken the interaction between the catalytic active species and nitrogen atom, which caused the product could be desorbed from the active center easily.[36] Compared with homogeneous hydrogenation of quinoline in Rh complex and Ru complex catalytic system,[37] the hydrogenation of quinoline was via an ionic and cascade reaction pathway through protonation of quinoline. In summary, the surface hydroxyl groups and water play a similar role to protonic acid and prevent the active center from the poison of quinoline as well as its hydrogenation products. The proposed mechanism of quinoline over Ru-SiO_2@mSiO_2 is summarized in Scheme 4.

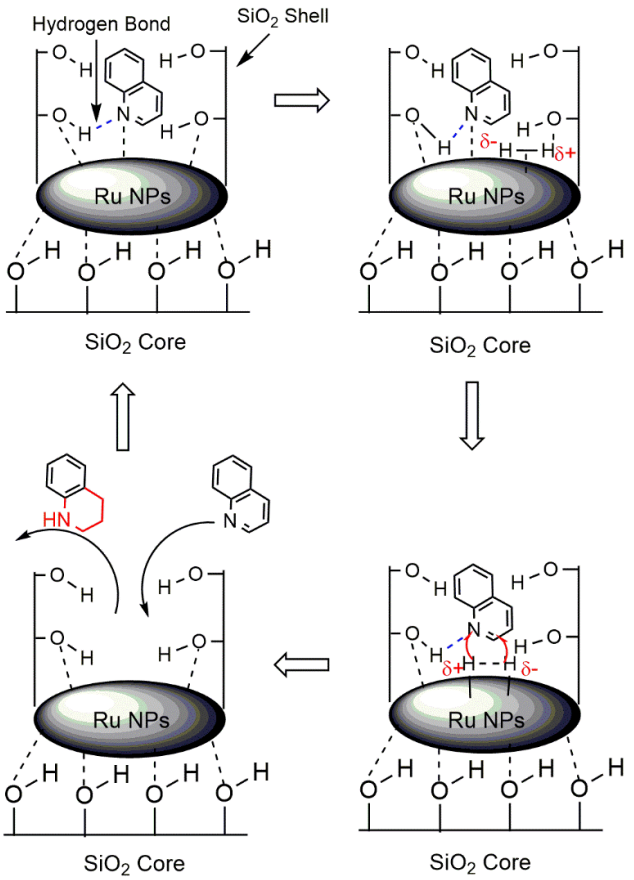

Scheme 4 The possible catalytic mechanism of quinoline over Ru-SiO_2@mSiO_2 catalyst

The mechanism described in Scheme 4 was further supported by IR spectrum, ^{13}C solid-state NMR spectrum, and theory calculation. The IR spectra of quinoline, catalyst and quinoline adsorbed on the catalyst were illustrated in Fig. 6.

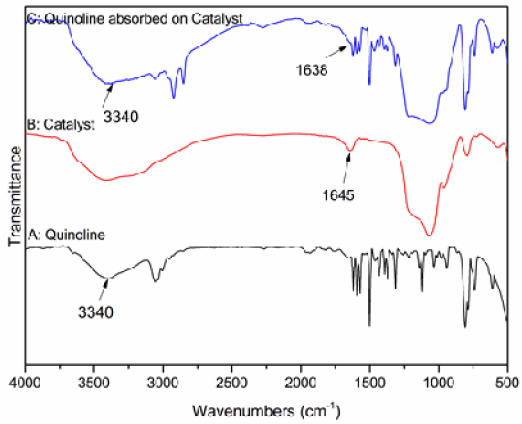

Fig. 6 The IR spectrum of quinoline, catalyst and quinoline absorption on catalyst

The absorption peak at 1645 cm^{-1} in Fig. 6B was attributed to the flexural vibration of hydroxyl groups of the catalyst. After the catalyst adsorbed quinoline (Fig. 6C), the absorption peak was red-shifted to 1638 cm^{-1} due to the formation of hydrogen bond between the nitrogen atom and the hydroxyl group. Also the peak at 3340 cm^{-1} was broaden after mixed with quinoline (Fig. 6C) because of the formation of hydrogen bond between N atom and the hydroxyl group on the catalyst.[38] In that case, the hydrogen bond weakened the O-H bond of hydroxyl groups on the catalyst surface obviously. As a comparison, the flexural vibrations of O-H bond at the peak of about 1645 cm^{-1} did not almost change while the peak at 3340 cm^{-1} did not broaden when quinoline was absorbed on the catalysts denominated as Ru/SiO_2 and Ru/SiO_2-spheres (Fig. S9, ESI). It is proved that a strong hydrogen bond quinoline and the surface hydroxyl group of Ru-SiO_2@mSiO_2 is present. Also, the solid-stated ^{13}C CP/MAS NMR was used to detect the chemical shift of the carbon atom marked as C (1). The NMR spectra of the free quinoline, quinoline adsorbed on the silica, and quinoline adsorbed on the catalyst were shown in Fig. 7.

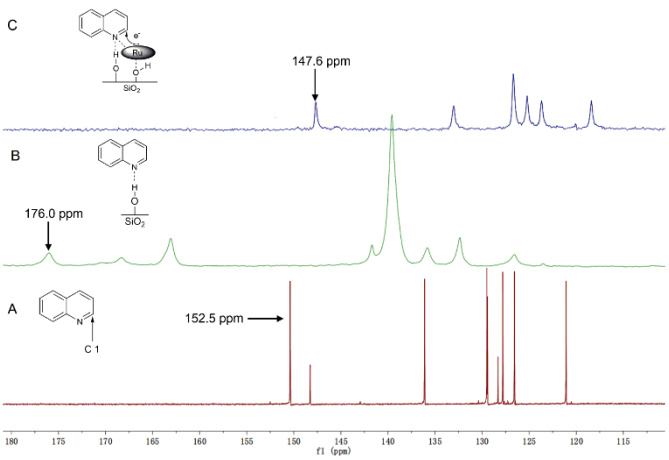

Fig. 7 The ^{13}C NMR of quinoline (A) and ^{13}C CP/MAS NMR of quinoline absorbed on the silica spheres (B) and catalyst (C)

The singlet at 152.5 ppm was attributed to C (1) in free quinoline (Fig. 7A), which was shifted to 176.0 ppm (Fig. 7B) after quinoline was adsorbed on silica. This phenomena was attributed to the formation of hydrogen bond between nitrogen atom and hydroxyl group on the silica, which decreased the electronic cloud density of C (1) atom via inductive electronic effect. The chemical shift for C (1) was shifted to 147.6 ppm after quinoline was of absorption on the catalyst (Fig. 7C). The d electrons of the Ru species could back-donate to quinoline through the coordination of nitrogen atom with Ru species, which resulted in the increase of electronic cloud density and also caused the chemical shift was moved to upfield. ^{13}C CP/MAS NMR was also used to test the C (1) chemical shift of quinoline absorbed on Ru/SiO_2 (Fig. S10A, ESI) and Ru/SiO_2-spheres (Fig. S10B, ESI). The chemical shift of C (1) was displayed at 151.0 ppm in Fig. S10A and 149.0 ppm in Fig. S10B, which was higher than 147.6 ppm on the Ru-SiO_2@mSiO_2. That was to say, the weak interaction between quinoline and Ru/SiO_2 or Ru/SiO_2-spheres led to less d electrons back-donating to quinoline. In that case, the quinoline could not be activated efficiently in the reaction by using Ru/SiO_2 and Ru/SiO_2-spheres as the catalyst. So the NMR results explained clearly the activity order of Ru-SiO_2@mSiO_2 > Ru/SiO_2-spheres > of Ru/SiO_2 (Table 3).

Theoretically evaluation (The calculation method was described in ESI) also provided more evidence for the proposed catalytic mechanism. The optimized states of quinoline and the absorption quinoline of on the silica were displayed in Fig. 8.

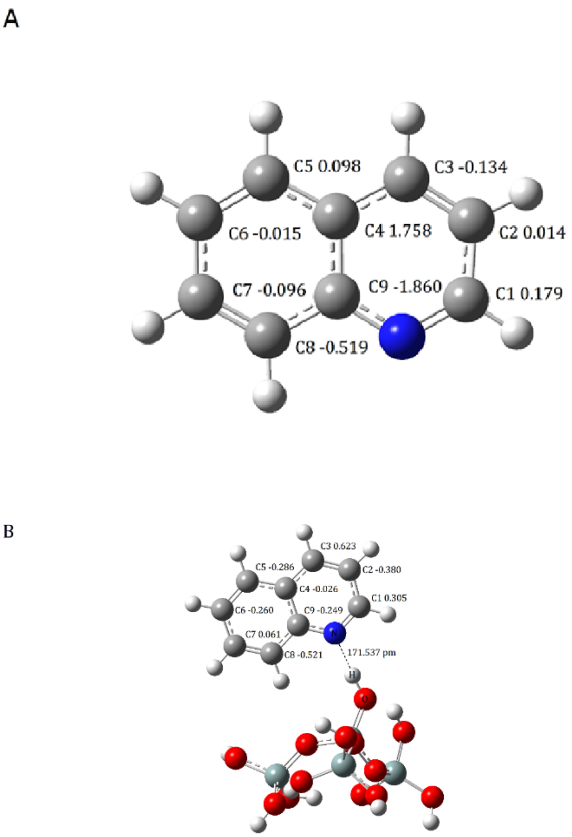

Fig. 8 The optimization of quinoline and quinoline absorbed on the silica with charge distribution

The charge distribution of carbon atoms in the quinoline optimization was outlined (Fig. 8A). The positive charge density of C (1) in free quinoline was calculated as 0.179 e. The positive charge density on C (1) was increased to 0.305 e after quinoline was absorbed on the silica which was optimizated to

the final state (Fig. 8B). The increase of positive charge density revealed that the electronic cloud deviated from C (1) atom through N-H...O interaction, which was an evidence for the formation of hydrogen bond. The O-H flexural vibration of the catalyst was calculated as 1650 cm^{-1} while the flexural vibration of O-H was shifted to 1647 cm^{-1} after the adsorption of quinoline on the catalyst. The tendency of adsorption peak agreed with experimental IR spectra. The results proved the presence of hydrogen bond between quinoline and the hydroxyl group. The ^{13}C NMR chemical shifts of C (1) atom in free quinoline and the absorption of quinoline on silica through the hydrogen bond between nitrogen atom and surface hydroxyl group were calculated as 155 ppm and 168.6 ppm, which was of good agreement with the experimental NMR spectra. It was a powerful evidence for the presence of the hydrogen bond. While the quinoline was absorbed on Ru-SiO_2@mSiO_2, the length of the bond between N-C (1) was increased from 131.874 pm to 132.147 pm due to the formation of N···H-O hydrogen bond, which was calculated as 171.537 pm. The increase of the length of N-C (1) bond and the presence of the N···H-O hydrogen bond suggested that the quinoline molecule was efficiently activated in this catalytic system.

3.2.6 Test for other substrates

Later, the hydrogenation of more substrates was carried out smoothly over Ru-SiO_2@mSiO_2 and the results were summarized in Table 4.

Table 4 Hydrogenation of other substrates over Ru-SiO_2@mSiO_2

Substrates	Product	Solvent	Temp. (K)	Time (h)	Conv.[a] (%)	Sel.[a] (%)
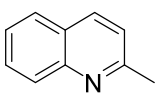	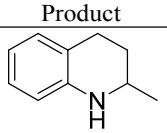	H_2O	363	5	100	100
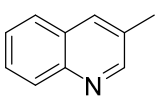	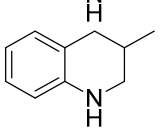	H_2O	363	5	100	100
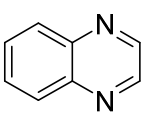	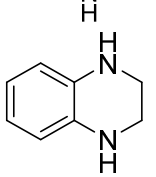	H_2O	363	5	90.3	100
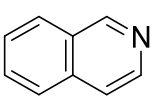	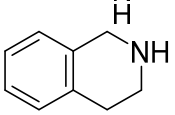	H_2O	363	5	87.5	100
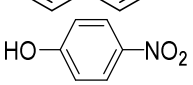	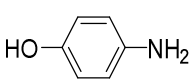	H_2O and Ethanol [b]	363	3	100	100
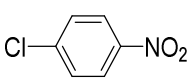	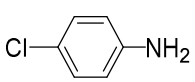	H_2O and Ethanol [b]	363	3	100	100

Reaction conditions: 1.0 mmoL substrate, Ru, 0.67 mol% relative to substrate; 2.0 mL solvent.
a. Determined by GC and GC–MS.
b.V(H_2O) :V(Ethanol) = 1:1

The complete conversion in the hydrogenation of 2-methylquinoline and 3-methylquinoline was achieved with the 100% selectivity to corresponding 1,2,3,4-tetrahydroquinolines. Also, in the hydrogenation of quinoxaline and isoquinoline, 90.3% and 87.5% of conversion with the 100% to 1,2,3,4-tetrahydroquinoxaline and 1,2,3,4-tetrahydroisoquinoline were obtained. For hydrogenation of *p*-chloronitrobenzene and 4-nitrophenol, both the conversion and selectivity were up to 100%. In Philippe Serp and coworkers' report, [1] nanostructured-carbon supported ruthenium catalysts were used for the hydrogenation of *p*-chloronitrobenzene. The selectivity to *p*-choroaniline was in the range of 92% to 94% due to dechlorination. So the catalyst could be widely applied in the hydrogenation of substrates containing nitrogen and oxygen atoms.

4. Conclusions

In summary, well dispersed Ru-SiO_2@mSiO_2 nanocomposite with BET surface area as high as 602 m^2/g has been prepared by a modified Stöber method. The as-synthesized catalyst shows great performance towards the hydrogenations of quinoline, *p*-chloronitrobenzene and 4-nitrophenol. Both the conversion of substrate and selectivity to the desired product are as high as 100% under mild conditions. For the hydrogenation of quinoline, the catalyst can be reused 5 times without any loss of the catalytic activity and selectivity to ^{1}THQ. It is suggested that the formation of hydrogen bond N···H-O between quinoline and the surface hydroxyl group of the catalyst facilitates the adsorption of N-heterocycle of quinoline. Furthermore, the hydrogen bond weakens the coordinate ability of nitrogen atom in quinoline and its hydrogenation derivatives with ruthenium, which results in the unprecedented recycling ability in our catalytic system. This study does suggest a new path to synthesize a novel kind of nanocatalyst with the high catalytic performance. Moreover, hydrogenation of quinoline catalyzed by Ru-SiO_2@mSiO_2 in water is "green processing" in terms of its environmental impact as it fulfills the majority of the green chemistry requirements [39] including the followings: (I) it is 100% conversion and selectivity to desired product and minimizes by-products or waste; (II) it maximizes the incorporation of all reactants into the products; (III) water is used as the solvent in the reaction to avoid using the toxic reagent; (IV) hydrogenation of quinoline in water is catalytic processing, not stoichiometric; (V) no blocking, protecting/deprotecting group was used in the catalytic processing.

5 Acknowledgements

We are grateful to the China National Natural Science Foundation (No. 21072138) and National Science Talents fund for research training and research ability improvement project (NO. j1103315)

Notes and Reference:

[a] Key lab of Green Chemistry and Technology, Ministry of Education; Sichuan University, Chengdu, China. Fax: 86-28-85412904; E-mail: liruixiang@scu.edu.cn

[b] Analytical &Testing Centre of College of chemistry, Sichuan University, China. E-mail: wangshanling@scu.edu.cn

† Footnotes should appear here. These might include comments relevant to but not central to the matter under discussion, limited experimental and spectral data, and crystallographic data.

Electronic Supplementary Information (ESI) available: [details of any supplementary information available should be included here]. See DOI: 10.1039/b000000x/

1. M. Oubenali, G. Vanucci, B. Machado, M. Kacimi, M. Ziyad, J. Faria, A. Raspolli-Galetti, P. Serp, *ChemSusChem* 2011, **4**, 950.
2. M. Campanati, A. Vaccari, O. Piccolo, *J. Mol. Catal. A: Chem.* 2002, **179**, 287.
3. M. Campanati, M. Casagrande, I. Fagiolino, M. Lenarda, L. Storaro, M. Battagliarin, A. Vaccari, *J. Mol. Catal. A: Chem.* 2002, **184**, 267.
4. J. Chen, F. Xue, H. Y. Fu, G. Y. Fan, M. L. Yuan, H. Chen, X. J. Li., *Chin. J. Catal.* 2007, **28**, 975.
5. R. M. Zhang, G. Y. Fan, C. Li, Y. Y. Wang, R. X. Li, H. Chen, X. J. Li., *Acta Phys. Chin. Sin.* 2008, **24**, 965.
6. C. Bianchini, V. D. Santo, A. Meli, S. Moneti, M. Moreno, W. Oberhauser, R. Psaro, L. Sordelli, F. Vizza, *J. Catal.* 2003, **213**, 47.
7. H. Mao, C. Chen, X. P. Liao, B. Shi, *J. Mol. Catal. A: Chem.* 2011, **341**, 51.
8. Y. T. Gong, P. F. Zhang, X. Xu, Y. Li, H. R. Li, Y. Wang, *J. Catal.* 2013, **297**, 272
9. S.W. Kim, M. Kim, W.Y. Lee, T. Hyeon, *J. Am. Chem. Soc.* 2002, **124**, 7642.
10. R. G. Chaudhuri, S. Paria, *Chem. Rev.* 2012, **112**, 2373.
11. J. Lee, J. C. Park, J. U. Bang, H. Song, *Chem. Mater.* 2008, **20**, 5839.
12. J. Ge, Q. Zhang, T. Zhang, Y. Yin, *Angew. Chem. Int. Ed.* 2008, **46**, 8924.
13. K. Jiang, H. X. Zhang, Y. Y. Yang, R. Mothes, H. Lang, W. B. Cai, *Chem. Commun.* 2011, **471**, 1924.
14. Y. H. Deng, Y. Cai, Z. K. Sun, J. Liu, C. Liu, J. Wei, W. Li, C. Liu, Y. Wang, D. Y. Zhao, *J. Am. Chem. Soc.* 2010, **132**, 8466.
15. L. Xu, Y. Ren, H. Wu, Y. Liu, Z. Wang, Y. Zhang, J. Xu, H. Peng, P. Wu, *J. Mater. Chem.* 2011, **21**, 10852.
16. S. Okada, K. Mori, T. Kamegawa, M. Che, H. Yamashita, *Chem. Eur. J.* 2011, **17**, 9047.
17. A. S. Reddy, S. Kim, H. Y. Jeong, S. Jin, K. Qadir, K. Jung, C. H. Jung, J. Y. Yun, J. Y. Cheon, J. M. Yang, S. H. Joo, O. Terasaki, J. Y. Park, *Chem. Commun.* 2011, **47**, 8412.
18. D. Rosario-Amorin, M. Gaboyard, R. Clerac, L. Vellutini, S. Nlate, K. Heuze, *Chem. Eur. J.* 2012, **18**, 3305.
19. M. Cargnello, J. J. Delgado Jaén, J. C. Hernández Garrido, K. Bakhmutsky, T. Montini, J. J. Calvino Gámez, R. J. Gorte, P. Fornasiero, *Science*, 2012, **337**, 713.
20. (a) V.Sridharan, P. A. Suryavanshi, J. C. Menéndez, *Chem. Rev.* 2011, **111**, 7157; (b) R. Rahi, M. Fang, A. Ahmed, R. A. Sánchez-Delgado, *Dalton Trans.* 2012, **41**, 14490.
21. Y. P. Sun, H. Y. Fu, D. L. Zhang, R. X. Li, H. Chen, X. J. Li, *Catal. Commun.* 2010, **12**, 188.
22. G. Y. Fan, L. Zhang, H. Y. Fu, M. L. Yuan, R. X. Li, H. Chen, X. J. Li, *Catal. Commun.* 2010, **11**, 451.
23. H. J. Jiang, H. B. Jiang, D. M. Zhu, X. L. Zheng, H. Y. Fu, H. Chen, R. X. Li, *Appl. Catal. A: Gen.* 2012, **351**, 445.
24. Y. F. Zhou, J. Wei, G. Y. Fan, H. Y. Fu, R. X. Li, H. Chen, X. J. Li, *Chem. Lett.* 2009, **38**, 1304.
25. W. J. Stöber, *Colloid Interface Sci.* 1968, **26**, 62.
26. G. Liu, J. Wang, T. Huang, X. Liang, Y. Zhang, H. Li, *J. Mater. Chem.* 2010, **20**, 1970.
27. *Handbook of X-ray Photoelectron Spectroscopy*, Perkin-Elmer Corporation, 1992.
28. R. A. Rajadhyaksha, S. L. Karwa, *Chem. Eng. Sci.* 1986, **41**, 1765.
29. S. Mukherjee, M. A. Vannice, *J. Catal.* 2006, **243**, 108.
30. R. A. Sánchez-Delgado, N. Machalaba, N. Ng-a-qui, *Catal. Commun.* 2007, **8**, 2115.
31. E. Baralt, S. J. Smith, J. Hurwitz, I. T. Horvath, R. H. Fish, *J. Am. Chem. Soc.* 1992, **114**, 5187.
32. F. Alonso, M. Yus, *Adv. Synth. Catal.* 2001, **343**, 188.
33. B. Sun, F. A. Khan, A. Vallat, S. F. Georg, *Appl. Catal. A: Gen.* 2013, **467**, 310.
34. H. Mao, C. Chen, X. P. Liao, B. Shi, *J. Mol. Catal. A: Chem.* 2011, **34**, 51.
35. H. Nagahara, M. Ono, M. Konishi, Y. Fukuoka, *Appl. Surf. Sci.* 1997, **121/122**, 448.
36. L. Zhang, B. Hu, H. Chen, X. J. Li, R. X. Li, *Acta Physico-Chimica Sinica* 2010, **26**, 2422.
37. (a) C. Wang, C. Li, X. Wu, A. Pettman, J. Xiao, *Angew. Chem. Int. Ed*, 2009, **48**, 6524; (b) T. L. Wang, L. G. Zhuo, Z. W. Li, F. Chen, Z. Y. Ding, Y. M. He, Q. H. Fan, J. F. Xiang, Z. X. Yu, A. S. C. Chan. *J.Am. Chem. Soc*. 2011 **133**, 9878
38. C. W. Oo, M. J. Kassim, A. Pizzi, *Ind. Crop. Prod.* 2009, **30**, 152.
39. M. Poliakoff, J. M. Fitzpatrick, T. R. Farren, P. T. Anastas, *Science* 2002, **297**, 807.